ARTICLE IN PRESS

Annals of Physics ▮ (▮▮▮▮) ▮▮▮–▮▮▮

Contents lists available at ScienceDirect

Annals of Physics

journal homepage: www.elsevier.com/locate/aop

Making structured metals transparent for ultrabroadband electromagnetic waves and acoustic waves

Ren-Hao Fan [a], Ru-Wen Peng [a,*], Xian-Rong Huang [b], Mu Wang [a]

[a] National Laboratory of Solid State Microstructures and School of Physics, Collaborative Innovation Center of Advanced Microstructures, Nanjing University, Nanjing 210093, China

[b] Advanced Photon Source, Argonne National Laboratory, Argonne, IL 60439, USA

HIGHLIGHTS

- Making structured metals transparent for ultrabroadband electromagnetic waves.
- Non-resonant excitation of surface plasmons or spoof surface plasmons.
- Sonic artificially metallic structures transparent for broadband acoustic waves.

ARTICLE INFO

Article history:
Received 13 October 2014
Received in revised form
5 December 2014
Accepted 9 December 2014
Available online xxxx

Keywords:
Transparent structured metals
Broadband metamaterials
Transmission of electromagnetic waves and acoustic waves

ABSTRACT

In this review, we present our recent work on making structured metals transparent for broadband electromagnetic waves and acoustic waves via excitation of surface waves. First, we theoretically show that one-dimensional metallic gratings can become transparent and completely antireflective for extremely broadband electromagnetic waves by relying on surface plasmons or spoof surface plasmons. Second, we experimentally demonstrate that metallic gratings with narrow slits are highly transparent for broadband terahertz waves at oblique incidence and high transmission efficiency is insensitive to the metal thickness. Further, we significantly develop oblique metal gratings transparent for broadband electromagnetic waves (including optical waves and terahertz ones) under normal incidence. In the third, we find the principles of broadband transparency for structured metals can be extended from one-dimensional metallic gratings to

* Corresponding author.
E-mail address: rwpeng@nju.edu.cn (R.-W. Peng).

http://dx.doi.org/10.1016/j.aop.2014.12.029

Please cite this article in press as: R.-H. Fan, et al., Making structured metals transparent for ultrabroadband electromagnetic waves and acoustic waves, Annals of Physics (2015), http://dx.doi.org/10.1016/j.aop.2014.12.029

two-dimensional cases. Moreover, similar phenomena are found in sonic artificially metallic structures, which present the transparency for broadband acoustic waves. These investigations provide guidelines to develop many novel materials and devices, such as transparent conducting panels, antireflective solar cells, and other broadband metamaterials and stealth technologies.

1. Introduction

Making metals transparent for white light, which could achieve various fascinating applications in optoelectronics, has been expected for a long period. Bulk metals are naturally opaque to light due to the large index mismatch between metals and dielectrics. In recent years, by introducing artificial structures, it becomes possible to achieve transparent metals beyond their natural characteristics. For example, it has been found that surface plasmons (SPs) [1] or spoof surface plasmons (SSPs) [2] on the surface of structured metal can lead to extraordinary optical transmission [3–7]. Moreover, continuous (apertureless) metal films can become transparent due to the scattering cancellation mechanism [8,9]. Besides, electromagnetically induced transparency [10–12] can be realized by introducing metamaterials [13–25], which are constructed by metallic micro- and nano-structures. However, due to the underlying resonance mechanisms, all of these transparency phenomena occur only within very narrow frequency band, and the transmission efficiency is usually low for thick materials.

Fortunately, in 2010 we theoretically found for the first time [26] and later experimentally demonstrated [27] that metallic gratings can be made transparent for extremely broadband electromagnetic waves under oblique incidence. This unusual phenomenon can be understood either by our non-resonant excitation mechanism of SPs or SSPs on microscopic level [26–29] or by the anomalous impedance-matching mechanism from Alú's group [30–32]. For technological applications the oblique incidence geometry is inconvenient. To solve this problem, we have developed oblique metal gratings to achieve broadband transparence at normal incidence [26,27,33]. Besides, adiabatically tapered slits have been proposed to widen the angular range of incidence [34]. These structured metal microstructures have presented significant transparency and can be applied for conducting panels [9,35,36], white-beam polarizers [37], anti-reflective solar cells [28,38], etc.

Metallic gratings can also become completely transparent for acoustic waves [39,40]. Since acoustic waves are longitudinal waves without polarization, we may achieve white-beam full transmission and antireflection. This may open up a new field for various novel applications of acoustic gratings, including extraordinary acoustic transmission (EAT) [41], sub-wavelength sonic imaging and screening [42,43], grating interferometry, antireflection cloaking, Talbot effect-based phase contrast imaging [44], crack detection, and various other acoustic device applications.

In this review, we present our recent work on making structured metals transparent for broadband electromagnetic waves and acoustic waves via excitation of surface waves. We theoretically and experimentally show that one-dimensional (1D) and two-dimensional (2D) metallic gratings can become transparent and completely antireflective for extremely broadband electromagnetic waves by relying on surface plasmons or spoof surface plasmons. Similar phenomena are found in sonic artificially metallic structures, which present broadband transparency for acoustic waves. And a brief perspective on future work is also given. The investigations provide guidelines to develop novel broadband electromagnetic and sonic materials and devices.

2. Making one-dimensional metallic grating transparent for ultrabroadband electromagnetic waves

In this section, we show that one-dimensional metallic gratings can become transparent and completely antireflective for extremely broadband electromagnetic waves under oblique incidence

Please cite this article in press as: R.-H. Fan, et al., Making structured metals transparent for ultrabroadband electromagnetic waves and acoustic waves, Annals of Physics (2015), http://dx.doi.org/10.1016/j.aop.2014.12.029

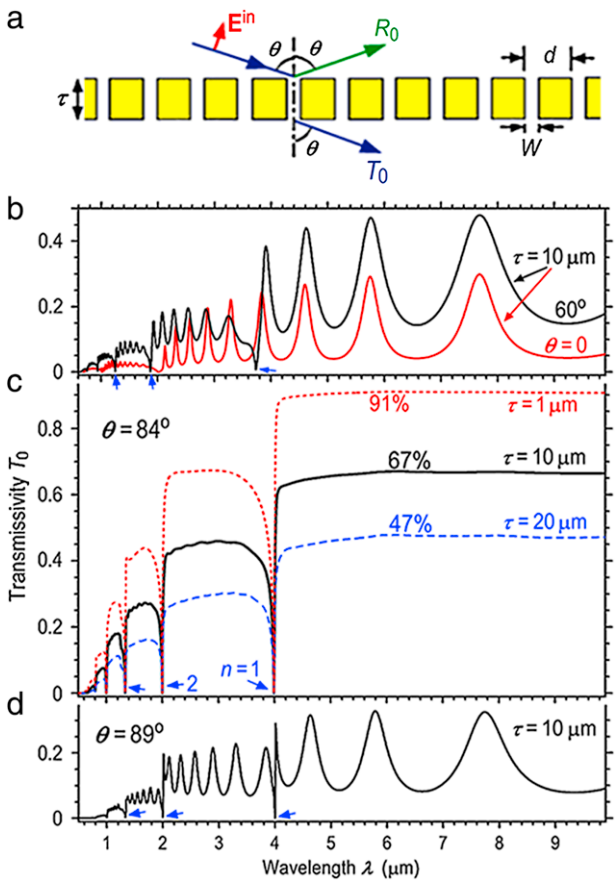

Fig. 1. (a) Schematic of the one-dimensional metal grating. Transmission spectra of a gold grating with $d = 2$ μm and $W = 0.2$ μm when TM polarization: (b) transmission for normal and 60° incidence, (c) maximized and flat transmission at $\theta = 84°$, (d) transmission for extremely grazing geometry.
Source: Partially adapted from [26].

when transverse magnetic polarization [26,27]. This unusual finding can be successfully explained by non-resonant excitation mechanism of SPs or SSPs on microscopic level [26]. It is known that SPs and SSPs are widely used in the fields such as surface-enhanced Raman scattering (SERS) [45], filters and waveguides [46,47] and so on.

The simple one-dimensional periodic slit arrays we studied is illustrated in Fig. 1(a) with d, W, and τ denoting the grating period, the slit width, and the grating thickness, respectively. Fig. 1(b) shows the calculated transmission curves computed by the rigorous coupled-wave analysis (RCWA) [48–50] of a gold grating with the incident angle $\theta = 0°$ and $\theta = 60°$ at $\tau = 10$ μm. The transmission peaks are well known to be Fabry–Perot (FP) resonance peaks [4,48,51,52]. In Fig. 1(b), one can see that the overall transmissivity T_0 increases with increasing incident angle θ. When θ is further increased to be around 84°, as shown in Fig. 1(c), it becomes more surprising that the FP peaks disappear and that the transmission curve becomes nearly flat in the long wavelength range $\lambda > d(1 + \sin\theta) \approx 2d$, the grating becomes transparent for a white beam. In Fig. 1(d), when θ is further increased towards 90°, T_0 drops again with the FP peaks reappearing.

This ultrabroadband transparence can be understood from the microscopic mechanism of light transmission through the slits with the assistance of free electron oscillation. For the scenario of normal incidence and FP resonance, where the charge densities at the four corners reach the maximum

Please cite this article in press as: R.-H. Fan, et al., Making structured metals transparent for ultrabroadband electromagnetic waves and acoustic waves, Annals of Physics (2015), http://dx.doi.org/10.1016/j.aop.2014.12.029

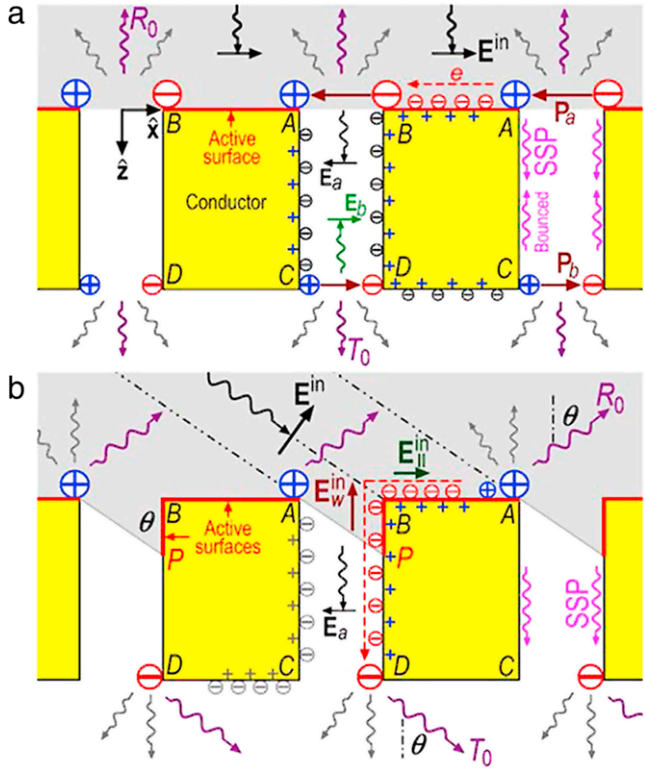

Fig. 2. Light transmission through conducting gratings. (a) Normal incidence. (b) Oblique incidence under the flat transmission condition.
Source: Partially adapted from [26].

as shown in Fig. 2(a). The incident electric field $\mathbf{E}_{in}$ drives the movement of free electrons on the top surface *AB* to form an oscillating dipole $\mathbf{P}_a$. $\mathbf{P}_a$ emits a wavelet inside the slit to form downward-propagating SPs. When the SPs reach the bottom, the charge movement is discontinued at corners *C* and *D* to form another oscillating dipole $\mathbf{P}_b$. Thus, $\mathbf{P}_a$ and $\mathbf{P}_b$ eventually form FP resonance under the condition $N\lambda \approx 2\tau$, where $N > 0$ is an integer and λ is the wavelength of the incident light [26]. The wavelets emitted from the periodic dipoles $\mathbf{P}_b$ along the forward direction to form the transmitted beam. The FP resonance depends on the grating thickness.

For the oblique incidence, as illustrated in Fig. 2(b), the incident beam directly illuminates part of the slit wall (*BP*), thus applies a vertical driving force $e\mathbf{E}_w$ on the electrons on the slit wall (*e* denotes the charge per electron). When the total forces exerted on *AB* and *BP* are balanced, the electrons can move smoothly around corner *B* without charge accumulation. Then the charge waves formed on *AB* and *BP* may propagate continuously on the unilluminated wall *PD* to the bottom. With this balanced-force condition, the FP resonance does not occur and SP excitation occurs only on the active surface *AB* and *BP*, resulting in strong light transmission through the slits [26]. The SPs can freely propagate on the slit wall *PD* towards the bottom, which also gives the physical reason why the flat transmission process is insensitive to the grating thickness. By carrying out the detailed analytical analysis [26], we find that the transmission efficiency reaches the maximum at the optimal incidence angle:

$$\theta_f \approx \arctan\left(d/W - 1\right). \tag{1}$$

Besides, we would like to mention here that broadband transparency in metal gratings can also be explained as an effective Brewster-like effect based on impedance matching [30]. When the light illuminates the grating at critical incident angle, the effective impedance for the slit equals to the

Please cite this article in press as: R.-H. Fan, et al., Making structured metals transparent for ultrabroadband electromagnetic waves and acoustic waves, Annals of Physics (2015), http://dx.doi.org/10.1016/j.aop.2014.12.029

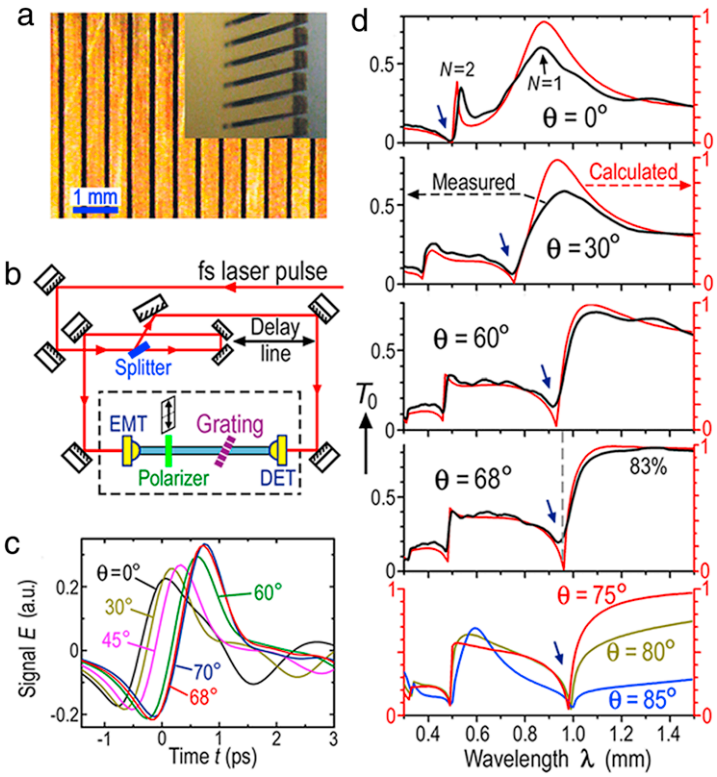

Fig. 3. Measurements and calculations of TM-polarization light transmission through a gold grating. (a) Optical image of the grating with period $d = 0.5$ mm, slit width $W = 0.15$ mm, and thickness $\tau = 0.34$ mm. The insert shows the cross section. (b) Schematic of the experiment setup. EMT: THz emitter. DET: THz detector. The dashed-line box is a nitrogen purging box. (c) Time-domain THz transmission signals for different incident angles. (d) Comparison of the measured and calculated transmission spectra.
Source: Partially adapted from [27].

impedance in free space. Thus the anomalous matching condition is achieved at so-called effective plasmonic Brewster angle [30]:

$$\cos\theta_B = (\beta_s w)/(k_0 d), \tag{2}$$

where β_s and k_0 are wave numbers in the slits and in the free space, respectively, w is slit width and d is period. This anomalous impedance-matching phenomenon is independent of the grating thickness.

3. Experimental demonstration of one-dimensional metallic grating transparent for ultrabroadband terahertz waves

In this section, we experimentally show that one-dimensional metallic gratings can become broadband transparence in the terahertz range [27], where the metals are highly conductive with negligible Ohmic loss.

The optical image of a gold grating is shown in Fig. 3(a). The measurements are carried out with an Ekspla THz real-time spectrometer, as schematically shown in Fig. 3(b). The time-domain signal $E(t)$ of the polychromatic terahertz pulse transmitted through the grating with different incident angles θ are shown in Fig. 3(c). Obviously, the grating is partially transparent at all the incident angles, and the signal amplitude increases as θ is approaching 68°. The transmittance spectra $T_0(\lambda)$ obtained from Fig. 3(c) by Fourier transformation are shown in Fig. 3(d). For comparison, we show also in Fig. 3(d)

Please cite this article in press as: R.-H. Fan, et al., Making structured metals transparent for ultrabroadband electromagnetic waves and acoustic waves, Annals of Physics (2015), http://dx.doi.org/10.1016/j.aop.2014.12.029

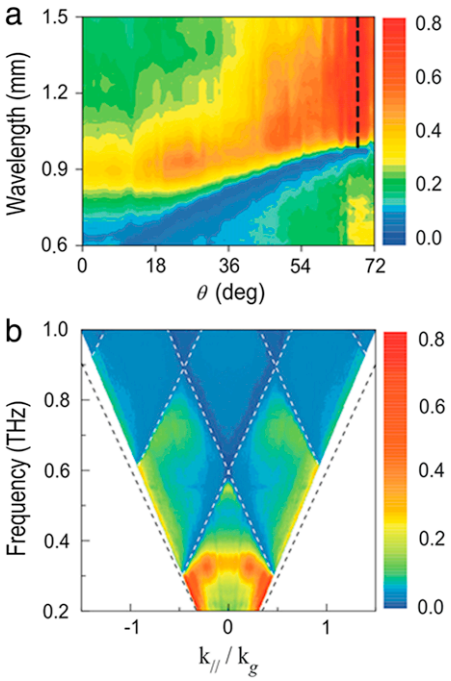

Fig. 4. (a) Experimentally measured angular transmission spectra of the gold grating with period $d = 0.5$ mm, slit width $W = 0.15$ mm, and thickness $\tau = 0.34$ mm. The black dashed line indicates the maximum transmission angles. (b) Experimentally measured dispersion map of this gold grating, black dotted lines represent light cone lines, white dotted lines show the position of Wood's anomaly. $k_{//} = 2\pi \sin\theta/\lambda$ is the in-plane wave vector, and $k_g = 2\pi/d$ is the reciprocal lattice vector. Color bar shows the measured transmission intensity. (For interpretation of the references to color in this figure legend, the reader is referred to the web version of this article.)
Source: Partially adapted from [27].

the corresponding spectra calculated by the RCWA method. The calculated maximum transmittance is nearly 100% due to the negligible Ohmic absorption of the grating. The measured maximum transmittance is about 83% which could be caused by the imperfections of the grating. Despite of the attenuation of the strength, the major features of the measured spectra are in good agreement with the calculations as shown in Fig. 3(d). For normal incidence $\theta = 0°$, the transmission peaks are known as FP resonance peaks. Beyond the FP resonance ranges, the transmission is very low. For oblique incidence, Fig. 3(d) shows that the long-wavelength transmission gradually increases as θ is increased. For $\theta = 68°$, the transmittance becomes nearly constant for $\lambda > \lambda_{WD1}$, $\lambda_{WD1}(\theta) = d(1 + \sin\theta)$ is the wavelength where the first-order Wood's anomaly occurs. The flat T_0 curves have little change in the range $67° < \theta < 72°$. The long-wavelength transmittance drops when $\theta > 75°$. Therefore, the angular range $67° < \theta < 75°$ is the maximum and nearly flat transmission range for this grating, which is close to the prediction of Eq. (1).

By measuring the optical spectra of oblique incidence from $\theta = 0$ to $\theta = 72°$, we obtain the angular transmission spectra and the dispersion map of the gold grating as shown in Fig. 4. It is evident that the maximum transmission appears around $\theta = 68°$, as marked by the dashed lined in Fig. 4. Broadband high transparency indeed occurs in the range $67° < \theta < 72°$. Therefore, we confirm the experiments that metallic gratings become highly transparent for broadband long wavelengths larger than the first-order Wood's anomaly with oblique incidence [27].

Actually the 1D metallic gratings with extreme subwavelength slit arrays can also become broadband transparence at microwave regime. Aközbek et al. [31] has experimentally found thick aluminum gratings can exhibit ultrabroadband, nearly perfect transmission at the plasmonic Brewster angle. They have demonstrated that the aluminum grating with period 3.6 mm, slit width 400 μm, and

Please cite this article in press as: R.-H. Fan, et al., Making structured metals transparent for ultrabroadband electromagnetic waves and acoustic waves, Annals of Physics (2015), http://dx.doi.org/10.1016/j.aop.2014.12.029

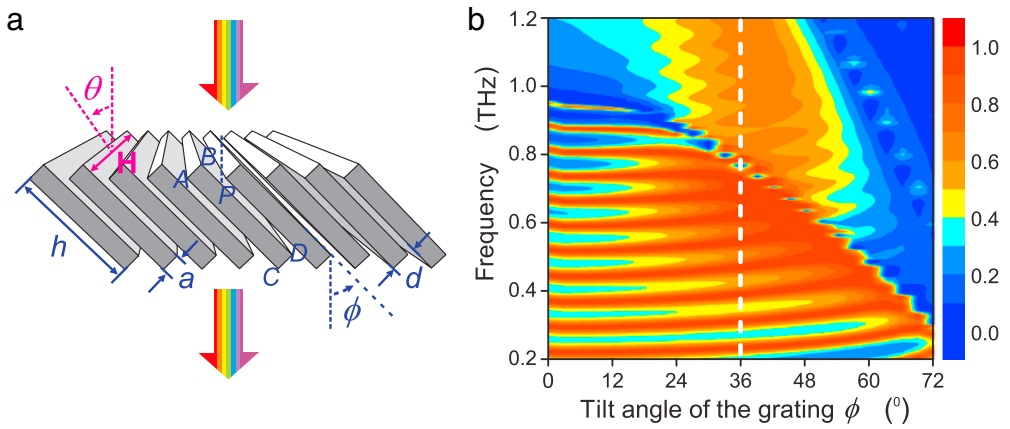

Fig. 5. (a) Schematic of the oblique metal grating. (b) Calculated normal-incidence ($\theta = 0^\circ$) transmission contour for oblique metal gratings with different tilt angles ϕ. $d = 305$ μm, $a = 200$ μm, and $h = 1.95$ mm. The white dashed line shows the optimal tilt angle determined by Eq. (2). The color bar shows the transmission intensity. (For interpretation of the references to color in this figure legend, the reader is referred to the web version of this article.)
Source: Partially adapted from [33].

thickness 2.54 cm can obtain high transmission at incident angle around 80° within 8–40 GHz, which agrees well with Eqs. (1) and (2). By changing the filling ratio of the grating, the Brewster angle can be tuned, and this ultrabroadband transparency effect is much more robust to losses and absorption compared with lots of resonant mechanisms for anomalous transmission [31].

4. Oblique metal gratings transparent for broadband electromagnetic waves at normal incidence

With the assistance of surface plasmons, metallic gratings can become non-dispersively transparent to broadband electromagnetic waves for oblique incidence. However, the oblique-incidence geometry may be inconvenient for technological applications. To solve this problem, we have employed a oblique metal grating achieving broadband transparency under normal incidence [27]. And Shen and Maes [34] have proposed the linearly tapered metallic gratings, and successfully broadened the incident angle range. The tapering provides a gradual impedance variation from the entrance to the exit of the slits, leading to broad-band and wide-angle enhanced transmission in the infrared. In this section, we present the oblique metal grating achieving broadband transparency under normal incidence via the transmission mapping measurements and direct terahertz imaging [33].

The tilt angle ϕ of the oblique metal gratings should be optimized first with the balanced-force condition [26]. When the light illuminates the oblique metal grating illustrated in Fig. 5(a), the incident electric field $\mathbf{E}_{in}$ drives the movement of free electrons on the top surface *AB* and part of the slit wall *BP*, thus applying driving forces on the electrons to move on *AB* and *BP*. When the total forces exerted on *AB* and *BP* are balanced $F_{AB} = F_{BP}$, the electrons can move smoothly around corner *B* without charge accumulation. Then the charge waves formed on *AB* and *BP* may propagate continuously on the unilluminated wall *PD* to the bottom, resulting in strong light transmission through the slits. The optimal tilt angle ϕ_f can be expressed as [33]:

$$\tan\phi_f(1+\tan^2\phi_f)/(1+\tan\phi_f) = a/d. \tag{3}$$

Fig. 5(b) shows the calculated transmission spectra of the oblique metal gratings at normal incidence with different tilt angle ϕ, where the grating period, the strip width, and the strip thickness are fixed as $d = 305$ μm, $a = 200$ μm, and $h = 1.95$ mm, respectively. Obviously, high broadband transmission indeed occurs through the gratings that have tilt angles around $\phi_f = 36^\circ$, and this optimal angle agrees well with Eq. (3).

Please cite this article in press as: R.-H. Fan, et al., Making structured metals transparent for ultrabroadband electromagnetic waves and acoustic waves, Annals of Physics (2015), http://dx.doi.org/10.1016/j.aop.2014.12.029

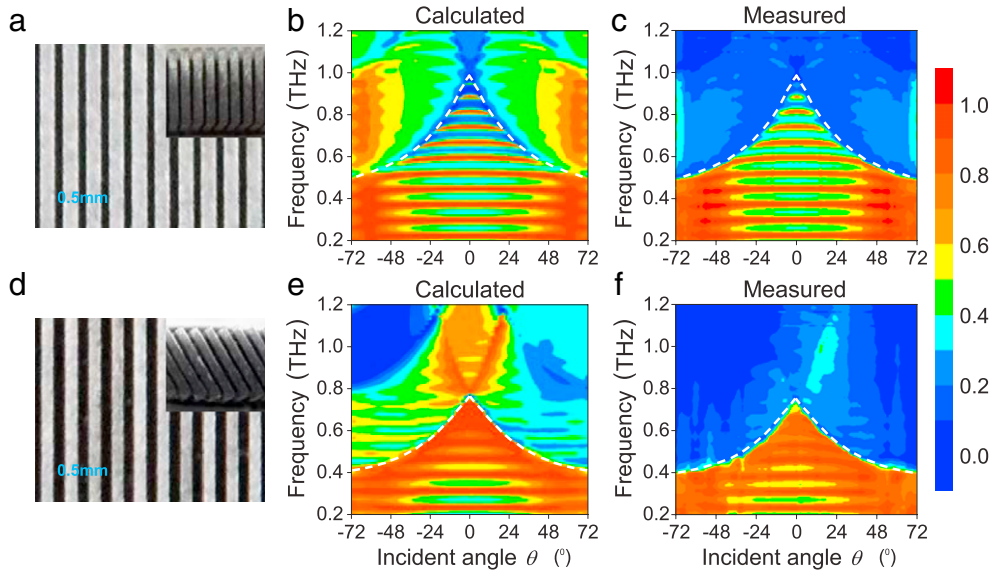

Fig. 6. (a) Photograph of the normal steel grating without tilt ($\phi = 0°$). Insert shows the cross section. (b) Calculated and (c) measured transmission spectra of the sample in (a). (d) Photograph of the oblique steel grating with $\phi = 36°$. (e) Calculated and (f) measured transmission spectra of the sample in (d). The white dashed lines correspond to the first-order Wood's anomalies. Color bar shows the transmission intensity. $d = 305$ μm, $a = 200$ μm, and $h = 1.95$ mm. (For interpretation of the references to color in this figure legend, the reader is referred to the web version of this article.)
Source: Adapted from [33].

We have used steel gratings to experimentally verify the above results. In our experiments, the gratings were assembled with steel strips. For comparison, we made two types of steel gratings with tilt angles $\phi = 0°$ and 36°, respectively, as shown in Fig. 6(a) and (d). Fig. 6(c) and (f) show the fine measurements of the optical transmission spectra for the incidence angle θ from −72° to 72° (with 1° step). For the normal grating ($\phi = 0°$), the first-order Wood's anomaly occurs at $f_{WD1}(\theta) = (c\cos\phi)/d(1+\sin\theta)$, which is marked by the white dashed line in Fig. 6. Nearly flat high transmission for frequency $f < f_{WD1}(\theta_f)$ can be observed when the incident angle is around $\theta_f \approx arctan[a/(d-a)] \approx 62°$ [26]. Obviously, this large incident angle is inconvenient for practical applications. As shown in Fig. 6(e) and (f), however, the oblique grating can achieve similar broadband high transmission under the more favorable normal-incidence condition $\theta = 0°$. For example, in Fig. 6(e) and (f) the normal-incidence transmission of the oblique grating can reach 80% within the wide band of 0.36–0.72 THz, which presents a nearly flat high transmission zone for the terahertz waves. As mentioned above, within this zone, the FP resonance is significantly suppressed and the average normal-incidence transmission intensity is obviously enhanced compared with that of the normal grating.

The high broadband transmission of oblique gratings can also be directly visualized by terahertz imaging techniques. As schematically shown in Fig. 7(a), our imaging experiments were carried out with the THz real-time spectrometer. In our experiments, the objects for imaging are three letters "N", "J", and "U" shown in Fig. 7(b), which were made from 0.2 mm-thick copper plates that are completely opaque to the terahertz beam. We have collected the images of the objects in the following cases. (i) No samples are before the objects. Fig. 7(c) shows the detected 2D images at frequency $f = 0.64$ THz. Naturally, the images clearly show the three-letter pattern ("NJU"), where dark-colored areas corresponds to low transmission and bright-colored areas to high transmission. (ii) A homogeneous 0.2-thick copper plate as the sample is placed before the objects. The 2D images are detected at the same frequency $f = 0.64$ THz (as shown in Fig. 7(d)). Obviously no patterns are observed on the images because the terahertz pulse cannot transmit through the copper plate.

Please cite this article in press as: R.-H. Fan, et al., Making structured metals transparent for ultrabroadband electromagnetic waves and acoustic waves, Annals of Physics (2015), http://dx.doi.org/10.1016/j.aop.2014.12.029

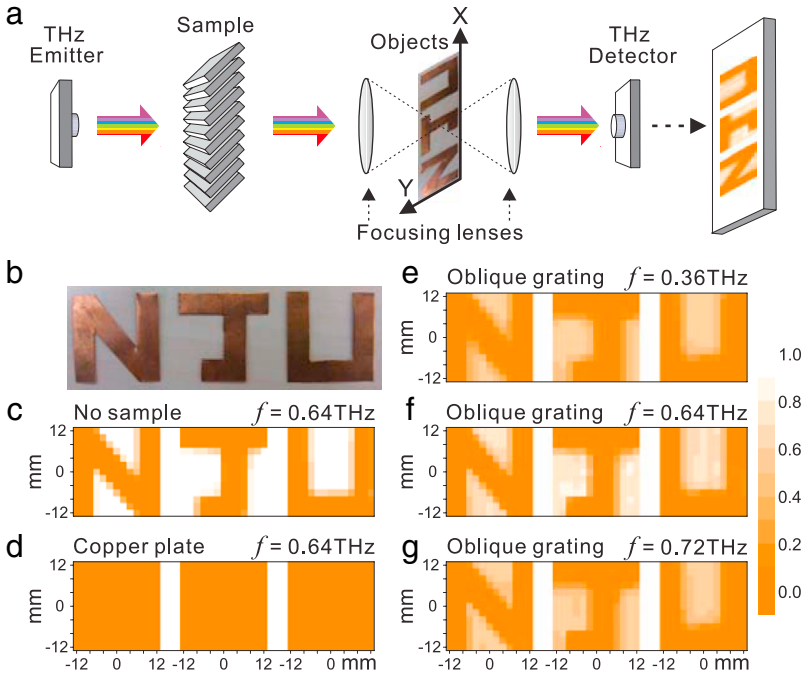

Fig. 7. (a) Schematic of the THz imaging system. (b) Photograph of the objects for imaging. (c) Detected images with no grating before the objects, $f = 0.64$ THz. (d) Blank images with a 0.2 mm-thick copper plate placed at the "Sample" position, $f = 0.64$ THz. (e)–(g) Images recorded with an oblique steel grating ($d = 305$ μm, $a = 200$ μm, $h = 1.95$ mm, and $\phi = 36°$) at the "Sample" position for different frequencies: (e) $f = 0.36$ THz, (f) $f = 0.64$ THz, and (g) $f = 0.72$ THz. Color bar shows the transmission intensity. (For interpretation of the references to color in this figure legend, the reader is referred to the web version of this article.)
Source: Adapted from [33].

(iii) Our oblique steel grating ($\phi = 36°$) as the sample is placed before the objects. The 2D images are detected at the frequency $f = 0.36$ THz, $f = 0.64$ THz, and $f = 0.72$ THz, respectively (as shown in Figs. 7(e)–(g)). It is shown that the pattern "NJU" of the objects is displayed very well in all three 2D images. Therefore, the 2D images clearly reveal the broadband transparency feature of the oblique metal gratings in the terahertz region.

5. Making two-dimensional metallic structures transparent for ultrabroadband electromagnetic waves

In this section, we extend the principles of ultrabroadband transmission from one-dimensional metallic gratings to the two-dimensional cases for both transverse-magnetic (TM) and transverse-electric (TE) waves, where the 2D structures are periodic metallic cuboids on dielectric or semiconductor substrates in the optical frequency range [28].

The 2D periodic metallic cuboids we studied is schematically shown in Fig. 8(a), where a TM or TE wave is incident on the structure by an angle θ from the Z axis. A field-emission scanning-electron microscope (SEM) image of one sample is shown in Fig. 8(b) with $d_x = d_y = 450$ nm, $w_x = w_y = 150$ nm, and $h = 100$ nm. The experimentally measured transmission spectra under different incidence angles are shown in Fig. 8(c) and (d). When the incident wave is TM polarized, the first-order Wood's anomaly along X direction is $\lambda_{WDx1}(\theta) = n_s d_x(1 + \sin\theta)$, which shifts from d to $2d$ with increasing θ. The transmittivity increases from $\theta = 0°$ to $\theta = 64°$, and then slightly decreases when θ further increases towards 90°. In particular, the transmission spectra become nearly flat at $\theta = 64°$ for long wavelengths $\lambda > \lambda_{WDx1}$, and the experimentally measured flat transmittivity

Please cite this article in press as: R.-H. Fan, et al., Making structured metals transparent for ultrabroadband electromagnetic waves and acoustic waves, Annals of Physics (2015), http://dx.doi.org/10.1016/j.aop.2014.12.029

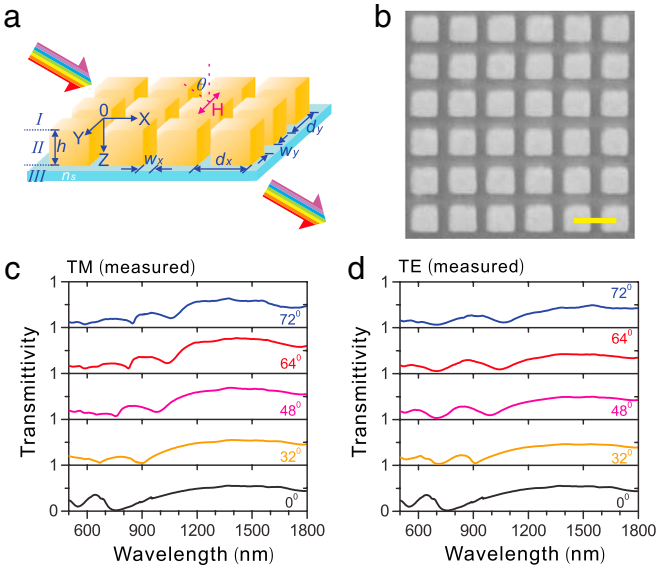

Fig. 8. (a) Schematic of metallic cuboids on the glass substrate. (b) SEM image of the sample, $d_x = d_y = 450$ nm, $w_x = w_y = 150$ nm, $h = 100$ nm, and $n_s = 1.47$. The scale bar is 500 nm. Measured transmission spectra at different incidence angles for (c) TM polarization and (d) TE polarization.
Source: Partially adapted from [28].

is nearly 80%. Therefore, the high ultrabroadband transmission in 2D periodic metallic cuboids for $\lambda > \lambda_{WDx1}$ is similar to that of the 1D metallic gratings under oblique incidence [26,27].

For TE polarization, significant transmission still occurs in Fig. 8(d) for long wavelengths $\lambda > \lambda_{WDx1}$. This is different from 1D metallic gratings, where TE waves are almost completely reflected in the long wavelength range. In Fig. 8(d), the transmission only slightly decreases with increasing θ from 0° to 90°. Therefore, the 2D periodic metallic cuboids are largely transparent also for TE waves in a wide angular range. This is a remarkable advantage for applications to solar cells that require transmission and antireflection of both TM and TE waves. These above experimental results are confirmed by numerical calculations based on the finite-difference time-domain (FDTD) method [53] with Lumerical FDTD Solution 8.0.1.

For different ratios of w_x/d_x along X axis, the maximum ultrabroadband transmission occurs around different optimal incident angles (θ_m). The calculated and measured θ-dependent TM transmission spectra with three different w_x/d_x ratios are shown in Fig. 9. The experimentally observed optimal angles are $\theta_m = 68°$ in Fig. 9(d) for $w_x/d_x = 0.25$, $\theta_m = 62°$ in Fig. 9(e) for $w_x/d_x = 0.375$, and $\theta_m = 56°$ in Fig. 9(f) for $w_x/d_x = 0.5$. Obviously, the angular ranges (areas) of the incident angle corresponding to high ultrabroadband transmission broaden when the radio w_x/d_x increases. For $w_x/d_x = 0.5$, significant transmission is observed in a wider angular range. Thus, we have demonstrated that high transmission and low reflection of 2D metallic cuboids can be achieved for both broad spectral bands and wide angular ranges.

In the following, we demonstrate that 2D periodic metallic cuboids can be used to design broad-angle and ultrabroadband solar cells based on the above high transmission and antireflection effect. Consider the structure of the solar cell in Fig. 10(a) that consists of three layers. On the top is a 2D periodic metallic cuboids made of aluminum. In the middle is a 20 nm-thick silicon oxide layer in order to avoid additional surface combination [38], below which is the semi-infinite single crystalline silicon layer acting as the absorber. In our design, the aluminum cuboids have the periods $d_x = d_y = 160$ nm, the gap widths $w_x = w_y = 80$ nm, and the thickness $h = 80$ nm. The total quantum efficiency enhancement [28] of this plasmonic solar cell can achieve 29.5%, which is even better than that of the traditional silicon solar cell using dielectric $\lambda/4$ AR coating as shown in Fig. 10(b). To see more,

Please cite this article in press as: R.-H. Fan, et al., Making structured metals transparent for ultrabroadband electromagnetic waves and acoustic waves, Annals of Physics (2015), http://dx.doi.org/10.1016/j.aop.2014.12.029

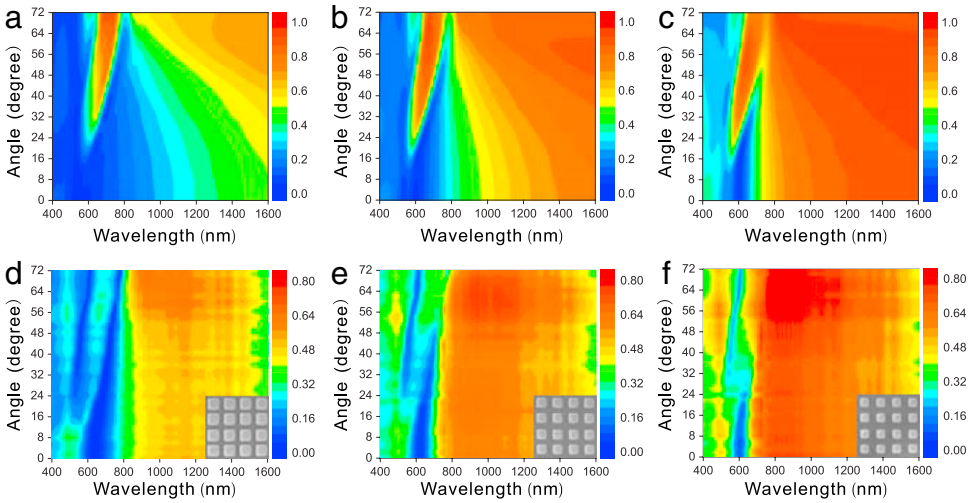

Fig. 9. Calculated angular transmission spectra for TM polarization: (a) $w_x = w_y = 80$ nm, (b) $w_x = w_y = 120$ nm, and (c) $w_x = w_y = 160$ nm. Experimentally measured angular transmission spectra for TM polarization: (d) $w_x = w_y = 80$ nm, (e) $w_x = w_y = 120$ nm, and (f) $w_x = w_y = 160$ nm. The color bar shows the transmission intensity. Insets show the SEM images of the corresponding samples. $d_x = d_y = 320$ nm, $h = 100$ nm, $n_s = 1.47$. (For interpretation of the references to color in this figure legend, the reader is referred to the web version of this article.)
Source: Partially adapted from [28].

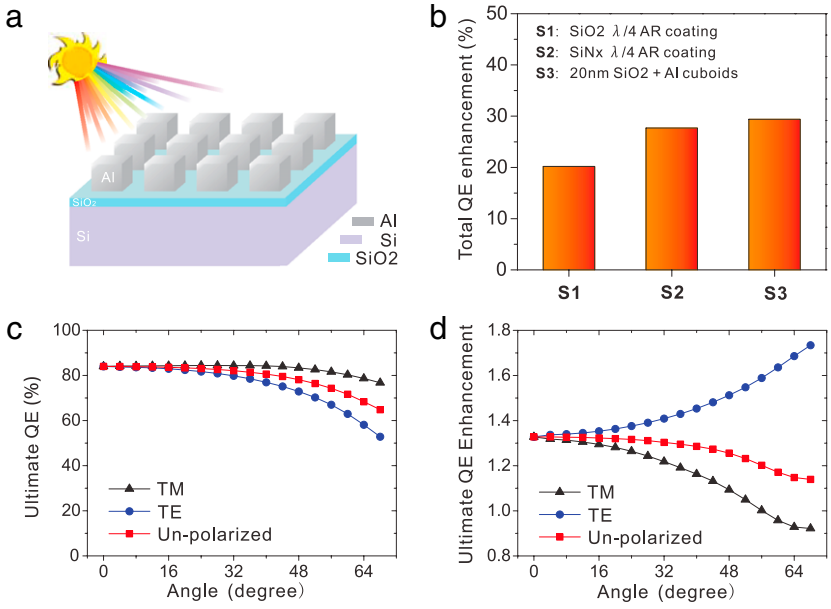

Fig. 10. (a) Schematic of the plasmonic solar cell that consists of three layers. On the top is a two-dimensional periodic metallic cuboids made of (low-cost) aluminum. In the middle is a 20 nm-thick silicon oxide layer, below which is the semi-infinite single crystalline silicon layer acting as the absorber. (b) The total quantum efficiency enhancement of three types of silicon solar cells. S1 is the cell with 100 nm-thick SiO_2 AR coating; S2 is the cell with 70 nm-thick SiNx AR coating; and S3 is the plasmonic solar cell with 2D Al cuboids. (c) The ultimate quantum efficiency (QE) of the plasmonic solar cell for different polarizations. (d) The ultimate QE enhancement for different polarizations. Here the parameters for 2D Al cuboids are $d_x = d_y = 160$ nm, $w_x = w_y = 80$ nm, and $h = 80$ nm.
Source: Partially adapted from [28].

Please cite this article in press as: R.-H. Fan, et al., Making structured metals transparent for ultrabroadband electromagnetic waves and acoustic waves, Annals of Physics (2015), http://dx.doi.org/10.1016/j.aop.2014.12.029

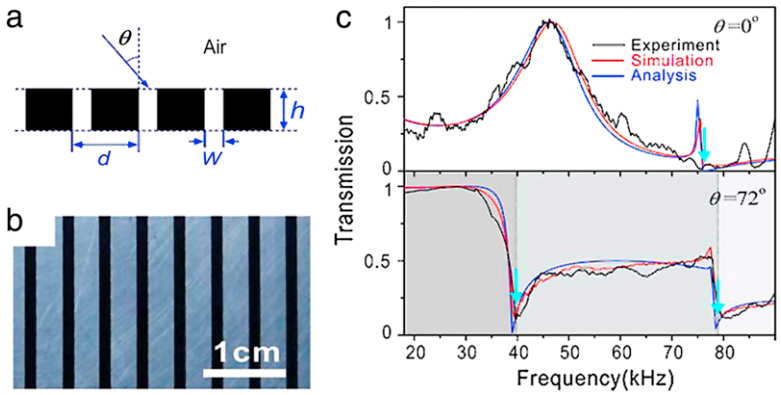

Fig. 11. (a) A schematic picture of a metallic grating. (b) The optical image of an experimental steel grating, where the period and the width of the slits are $d = 4.5$ mm and $w = 1.4$ mm, respectively, and the thickness of the grating is $h = 2.76$ mm. (c) Transmission spectra of this grating sample at normal incidence $\theta = 0^\circ$ and optimal incidence $\theta = 72^\circ$.
Source: Partially adapted from [39].

we calculated the ultimate quantum efficiency (QE) [54,55] of this plasmonic solar cell. The ultimate QE in Fig. 10(c) is high within the wavelength range 400–1000 nm. For TM polarization, the ultimate QE is greater than 84% in a wide angular range, and it only slightly decreases when θ is above 56°. Here the ultimate QE value for TM polarization is better than that of TE polarization due to the higher normalized absorbance in the semi-infinite single crystalline silicon layer, for unpolarized situation, the ultimate QE remains around 80% in a wide angular range. As shown in Fig. 10(d), its angle-dependent QE presents significant enhancement for all TM, TE, and unpolarized incident light, this is due to the fact that 2D periodic metallic cuboids have the properties of wide-angle and broadband antireflection.

6. Making metals transparent for ultrabroadband acoustic waves

In this section, we extend the transparence phenomena of structured metals for broadband acoustic waves, we find that metallic gratings can also be transparent for acoustic waves under oblique incidence within multiple frequency bands [39].

The sample we studied here is a 1D periodic steel grating as illustrated in Fig. 11(a). The optical image of a experimental steel grating is shown in Fig. 11(b), the period of the slits and the aperture size are $d = 4.5$ mm and $w = 1.4$ mm, respectively, and the thickness of the grating is $h = 2.76$ mm. The transmission spectra were measured by an analysis package of the 3560C Brüel & Kjær Pulse Sound and Vibration Analyzers [41]. Fig. 11(c) show the measured zero-order transmission spectra of the grating with normal incidence $\theta = 0^\circ$ and optimal incidence $\theta = 72^\circ$. For $\theta = 0^\circ$, at $f = 46.8$ kHz, the arrowed maximum transmission peak corresponds to the well known FP resonance peak. For θ increased to 72°, as show in Fig. 11(c), some interesting phenomena occur. The FP peaks disappear and the transmission curve becomes nearly flat, especially in the low frequency region, the transmission is nearly unit one and the grating is almost transparent for any frequency beam in that region. In high frequencies, the transmission curve decreases but still keep 'flat' pattern. With our simulations, we found that $\theta_f \sim 72^\circ$ is the critical incident angle with maximum and "flat" transmission for this steel gating.

To demonstrate the actual wave propagations through the gating, we calculated the spatial intensity distributions of the pressure field shown in Fig. 12(a) and (b). Though the transmissions of the two cases are both high, the intensity distributions are obviously distinguished. For $f = 47$ kHz with normal incidence, it is a typical FP resonant distribution. The intensity of the fields inside the gating is much larger than the incidence and transmitted waves. However, for $f = 34$ kHz with 72° incidence, the intensity of the field inside the apertures is in the same order of magnitude with the incidence and transmitted waves. It is apparent that the high transmission is not attributed to a resonant mechanism.

Please cite this article in press as: R.-H. Fan, et al., Making structured metals transparent for ultrabroadband electromagnetic waves and acoustic waves, Annals of Physics (2015), http://dx.doi.org/10.1016/j.aop.2014.12.029

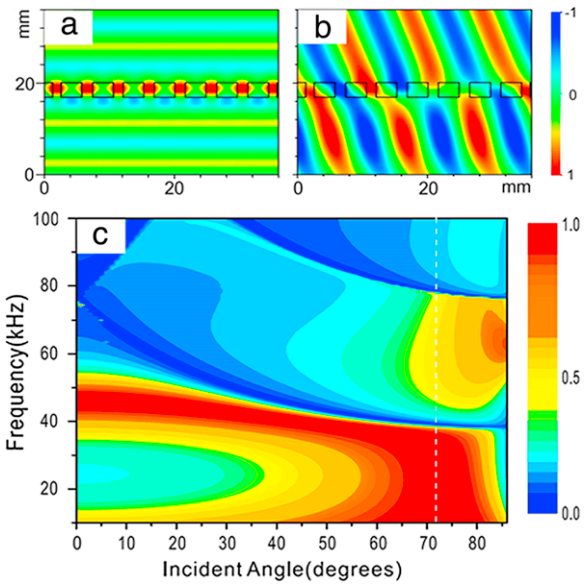

Fig. 12. The spatial intensity distribution of the pressure field (under periodic boundary) at high-transmission frequencies under different incident angles: (a) Normal incidence ($\theta = 0°$) at $\omega = 47$ kHz; (b) the optimal incidence ($\theta = 72°$) at $\omega = 34$ kHz. (c) The calculated angular transmission spectra of acoustic waves through the grating based on the RCWA method. The white dashed lines indicate the optimal incident angle $\theta_f = 71.7°$. The grating has the period of the slits $d = 4.5$ mm, the width of the slit $w = 1.4$ mm, and the thickness $h = 2.76$ mm.
Source: Partially adapted from [39].

The phenomenon originates from acoustic impedance match between the effective impedance of the grating and the impedance of air [39]. And high transmission in metal gratings happens at effective acoustic Brewster angle as [39]

$$\theta_B = \cos^{-1}(w/d). \tag{4}$$

In Fig. 12(c), we show the calculated acoustic transmission spectra of the thin grating versus different incident angles using this analysis model, the calculated acoustic Brewster angle θ_B equals to 71.7°, which is indicated by dashed line. When incident angle is small, the dark red region in Fig. 12(c) corresponds to the fundamental FP resonance peak, which has a small red shift with increasing incident angle. With θ increased to the predicted acoustic Brewster angle, FP peak is covered up by a broadband full transmission.

It is worthwhile to mention that D'Aguanno et al. [40] has found that not only 1D acoustic grating can transparent for broadband acoustic waves under oblique incidence, but also 2D acoustic grating has similar phenomenon, because sound waves are polarization independent which is different from electromagnetic waves. This ultrabroadband transparence for an acoustic metamaterial occurs at *intromission* angle [40], *i.e.*, $\cos\theta_I = S2/S1$, where $S2/S1$ represent the percentage of the open area of the screen. The nonresonant nature of the intromission tunneling separately arises at the entrance and exit of the screen, implying that is very robust to absorption or energy extraction for harvesting purposes within the apertures, and may be tailored to impedance match dissimilar media [40].

7. A brief perspective on future work

We have theoretically and experimentally shown that one-dimensional and two-dimensional metallic gratings can become transparent and completely antireflective for extremely broadband electromagnetic waves and acoustic waves. The physics underlying the transparency phenomena of

Please cite this article in press as: R.-H. Fan, et al., Making structured metals transparent for ultrabroadband electromagnetic waves and acoustic waves, Annals of Physics (2015), http://dx.doi.org/10.1016/j.aop.2014.12.029

electromagnetic and acoustic waves in structured metals may also shed new light on other waves, such as spin waves, fluid waves and even matter waves, in relevant structured materials.

Making metals transparent can lead to a variety of applications, including broadband transparent conducting panel, white-beam polarizers, antireflection materials, optical cloaking and stealth technologies, etc. Current studies mainly focus on some specific metallic structures, further work may extend to more complicated structural designing, and the state-of-the-art performance may be achieved in optimized metallic microstructures. Moreover, the physical concept on achieving broadband responses by relying on nonresonant mechanisms can further applied to develop other broadband metamaterials and broadband optodevices.

8. Conclusion

In this paper, we have reviewed our recent works on making structured metals transparent for broadband electromagnetic waves and acoustic waves. We have theoretically and experimentally presented that 1D and 2D metallic gratings can become transparent and completely antireflective for extremely broadband electromagnetic waves by relying on surface plasmons or spoof surface plasmons, the high transmission efficiency is insensitive to the metal thickness [26–28]. Further, we have significantly developed oblique metal gratings transparent for broadband electromagnetic waves (including optical waves and terahertz ones) under normal incidence [27,33]. Similar phenomena have also been found in sonic artificially metallic structures, which present the transparency for broadband acoustic waves [39]. The underlying physics broadens our understanding on interactions between photons [56] together with phonons [57] and microstructures. And these investigations also provide guidelines to develop many novel materials and devices, such as transparent conducting panels, white-beam polarizers, antireflective solar cells, and other broadband metamaterials and stealth technologies.

Acknowledgments

This work was supported by the Ministry of Science and Technology of China (Grant Nos. 2012CB921502 and 2010CB630705), and the National Natural Science Foundation of China (Grant Nos. 11034005, 61475070, and 11474157).

References

[1] W.L. Barnes, A. Dereux, T.W. Ebbesen, Nature 424 (2003) 824.
[2] J.B. Pendry, L. Martín-Moreno, F.J. Garcia-Vidal, Science 305 (2004) 847.
[3] T.W. Ebbesen, H.J. Lezec, H.F. Ghaemi, T. Thio, P.A. Wolff, Nature 391 (1998) 667.
[4] J.A. Porto, F.J. García-Vidal, J.B. Pendry, Phys. Rev. Lett. 83 (1999) 2845.
[5] Z.H. Tang, R.W. Peng, Z. Wang, X. Wu, Y.J. Bao, Q.J. Wang, Z.J. Zhang, W.H. Sun, Mu Wang, Phys. Rev. B 76 (2007) 195405.
[6] H. Liu, P. Lalanne, Nature 452 (2008) 728.
[7] Y.J. Bao, R.W. Peng, D.J. Shu, Mu Wang, X. Lu, J. Shao, W. Lu, N.B. Ming, Phys. Rev. Lett. 101 (2008) 087401.
[8] L. Zhou, W.J. Wen, C.T. Chan, P. Sheng, Phys. Rev. Lett. 94 (2005) 243905.
[9] Z.Y. Song, Q. He, S.Y. Xiao, L. Zhou, Appl. Phys. Lett. 101 (2012) 181110.
[10] S. Zhang, D.A. Genov, Y. Wang, M. Liu, X. Zhang, Phys. Rev. Lett. 101 (2008) 047401.
[11] N. Liu, L. Langguth, T. Weiss, J. Kästel, M. Fleischhauer, T. Pfau, H. Giessen, Nat. Mater. 8 (2009) 758.
[12] L. Qin, K. Zhang, R.W. Peng, X. Xiong, W. Zhang, X.R. Huang, Mu Wang, Phys. Rev. B 87 (2013) 125136.
[13] J.B. Pendry, Phys. Rev. Lett. 85 (2000) 3966.
[14] R.A. Shelby, D.R. Smith, S. Schultz, Science 292 (2001) 77.
[15] T.J. Yen, W.J. Padilla, N. Fang, D.C. Vier, D.R. Smith, J.B. Pendry, D.N. Basov, X. Zhang, Science 303 (2004) 1494.
[16] N. Fang, H. Lee, C. Sun, X. Zhang, Science 308 (2005) 534.
[17] J.B. Pendry, D. Schurig, D.R. Smith, Science 312 (2006) 1780.
[18] J.T. Shen, P.B. Catrysse, S. Fan, Phys. Rev. Lett. 94 (2005) 197401.
[19] J.B. Pendry, D. Schurig, D.R. Smith, Science 312 (2006) 1780.
[20] B. Zhang, Y.Y. Weng, X.P. Huang, Mu Wang, R.W. Peng, N.B. Ming, B. Yang, N. Lu, L. Chi, Adv. Mater. 21 (2009) 3576.
[21] X. Xiong, W.H. Sun, Y.J. Bao, R.W. Peng, Mu Wang, C. Sun, X. Lu, J. Shao, Z.F. Li, N.B. Ming, Phys. Rev. B 80 (2009) 201105(R).
[22] X. Xiong, W.H. Sun, Y.J. Bao, Mu Wang, R.W. Peng, C. Sun, X. Lu, J. Shao, Z.F. Li, N.B. Ming, Phys. Rev. B 81 (2010) 075119.
[23] M. Choi, S.H. Lee, Y. Kim, S.B. Kang, J. Shin, M.H. Kwak, K.Y. Kang, Y.H. Lee, N. Park, B. Min, Nature 470 (2011) 369.
[24] Y. Liu, X. Zhang, Chem. Soc. Rev. 40 (2011) 2494.
[25] J.Z. Zhao, D.L. Wang, R.W. Peng, Q. Hu, Mu Wang, Phys Rev E 84 (2011) 046607.
[26] X.R. Huang, R.W. Peng, R.H. Fan, Phys. Rev. Lett. 105 (2010) 243901.

Please cite this article in press as: R.-H. Fan, et al., Making structured metals transparent for ultrabroadband electromagnetic waves and acoustic waves, Annals of Physics (2015), http://dx.doi.org/10.1016/j.aop.2014.12.029

[27] R.H. Fan, R.W. Peng, X.R. Huang, J. Li, Y. Liu, Q. Hu, Mu Wang, X. Zhang, Adv. Mater. 24 (2012) 1980.
[28] R.H. Fan, L.H. Zhu, R.W. Peng, X.R. Huang, D.X. Qi, X.P. Ren, Q. Hu, Mu Wang, Phys. Rev. B 87 (2013) 195444.
[29] C. Meng, R.W. Peng, R.H. Fan, X.R. Huang, Mu Wang, Sci. China Inf. Sci. 56 (2013) 120404.
[30] A. Alù, G. D'Aguanno, N. Mattiucci, M.J. Bloemer, Phys. Rev. Lett. 106 (2011) 123902.
[31] N. Aközbek, N. Mattiucci, D. de Ceglia, R. Trimm, A. Alù, G. D'Aguanno, M.A. Vincenti, M. Scalora, M.J. Bloemer, Phys. Rev. B 85 (2012) 205430.
[32] K.Q. Le, C. Argyropoulos, N. Mattiucci, G. D'Aguanno, M.J. Bloemer, A. Alù, J. Appl. Phys. 112 (2012) 094317.
[33] R.H. Fan, J. Li, R.W. Peng, X.R. Huang, D.X. Qi, D.H. Xu, X.P. Ren, Mu Wang, Appl. Phys. Lett. 102 (2013) 171904.
[34] H. Shen, B. Maes, Appl. Phys. Lett. 100 (2012) 241104.
[35] X.P. Ren, R.H. Fan, R.W. Peng, X.R. Huang, D.H. Xu, Y. Zhou, Mu Wang, Phys. Rev. B 91 (2015) 045111.
[36] J.D. Edmunds, M.J. Lockyear, A.P. Hibbins, J.R. Sambles, I.J. Youngs, Appl. Phys. Lett. 102 (2013) 011120.
[37] P. Yeh, Opt. Commun. 26 (1978) 289.
[38] H.A. Atwater, A. Polman, Nat. Mater. 9 (2010) 205.
[39] D.X. Qi, R.H. Fan, R.W. Peng, X.R. Huang, M.H. Lu, X. Ni, Q. Hu, Mu Wang, Appl. Phys. Lett. 101 (2012) 061912.
[40] G. D'Aguanno, K.Q. Le, R. Trimm, A. Alù, N. Mattiucci, A.D. Mathias, N. Aközbek, M.J. Bloemer, Sci. Rep. 2 (2012) 340.
[41] D.X. Qi, Y.Q. Deng, D.H. Xu, R.H. Fan, R.W. Peng, Z.G. Chen, M.H. Lu, X.R. Huang, Mu Wang, Appl. Phys. Lett. 106 (2015) 011906.
[42] H. Estrada, P. Candelas, A. Uris, F. Belmar, F.J. García de Abajo, F. Meseguer, Phys. Rev. Lett. 101 (2008) 084302.
[43] T. Brunet, J.L. Thomas, R. Marchiano, Phys. Rev. Lett. 105 (2010) 034301.
[44] N. Saiga, Y. Ichioka, Appl. Opt. 24 (1985) 1459.
[45] H.X. Xu, E.J. Bjerneld, M. Käll, L. Börjesson, Phys. Rev. Lett. 83 (1999) 4357.
[46] Q. Hu, J.Z. Zhao, R.W. Peng, F. Gao, R.L. Zhang, Mu Wang, Appl. Phys. Lett. 96 (2010) 161101.
[47] Q. Hu, D.H. Xu, Y. Zhou, R.W. Peng, R.H. Fan, N.X. Fang, Q.J. Wang, X.R. Huang, Mu Wang, Sci. Rep. 3 (2013) 3095.
[48] X.R. Huang, R.W. Peng, J. Opt. Soc. Am. A 27 (2010) 718.
[49] P. Lalanne, G.M. Morris, J. Opt. Soc. Am. A 13 (1996) 779.
[50] B. Guizal, H. Yala, D. Felbacq, Opt. Lett. 34 (2009) 2790.
[51] X.R. Huang, R.W. Peng, Z. Wang, F. Gao, S.S. Jiang, Phys. Rev. A 76 (2007) 035802.
[52] F.J. Garcia-Vidal, L. Martin-Moreno, T.W. Ebbesen, L. Kuipers, Rev. Modern Phys. 82 (2010) 729.
[53] A. Taflove, S.C. Hagness, Computational Electrodynamics: The Finite-Difference Time-Domain Method, third ed., Artech House, Norwood, 2005.
[54] W. Shockley, H.J. Queisser, J. Appl. Phys. 32 (1961) 510.
[55] R.W. Peng, M. Mazzer, K.W.J. Barnham, Appl. Phys. Lett. 83 (2003) 770.
[56] S.C. Jiang, X. Xiong, Y.S. Hu, Y.H. Hu, G.B. Ma, R.W. Peng, C. Sun, Mu Wang, Phys. Rev. X 4 (2014) 021026;
X.R. Huang, D.P. Siddons, A.T. Macrander, R.W. Peng, X.S. Wu, Phys. Rev. Lett. 108 (2012) 224801.
[57] L.S. Cao, D.X. Qi, R.W. Peng, Mu Wang, P. Schmelcher, Phys. Rev. Lett. 112 (2014) 075505.

Please cite this article in press as: R.-H. Fan, et al., Making structured metals transparent for ultrabroadband electromagnetic waves and acoustic waves, Annals of Physics (2015), http://dx.doi.org/10.1016/j.aop.2014.12.029